Available online at www.sciencedirect.com
ScienceDirect
Journal of the European Ceramic Society 28 (2008) 691–698
www.elsevier.com/locate/jeurceramsoc

Oxidation behavior of AlN films at high temperature under controlled atmosphere

Chih-Yuan Lin, Fu-Hsing Lu *

Department of Materials Science and Engineering, National Chung Hsing University, 250 Kuo Kuang Road, Taichung 402, Taiwan

Received 7 May 2007; received in revised form 10 July 2007; accepted 20 July 2007
Available online 1 November 2007

Abstract

Oxidation behavior of AlN films deposited on Si substrates by unbalanced magnetron sputtering was investigated over temperatures of 700–1200 °C in different atmospheres by analyzing changes in appearance and crystalline phases, as well as microstructures. The atmospheres contained air, nitrogen, and forming gas ($N_2/H_2 = 9$), which exhibited drastically different nitrogen/oxygen partial pressure ratios. Observed color changes in appearance were associated with oxidation of the nitride film, which was analyzed by exploring Gibbs free-energy changes at various temperatures and nitrogen/oxygen partial pressures. Different phases of oxidants including intermediate δ-Al_2O_3 and thermodynamically stable α-Al_2O_3 were discerned by X-ray diffraction. Oxidation of AlN and phase transformation in Al_2O_3 depended on not only the temperature but the nitrogen/oxygen partial pressures. Microstructures of both oxide phases could be resolved by micro-Raman spectroscopy.

Keywords: AlN; Thin films; Oxidation; Al_2O_3; Phase changes; Microstructure

1. Introduction

Aluminum nitride (AlN) has been widely used in many electronic and opto-electronic applications owing to its excellent physical and chemical properties, such as high chemical stability and thermal conductivity (100–260 W/m K).[1,2] Moreover, *c*-axis oriented aluminum nitride exhibiting considerably high surface acoustic wave velocity (5070–5120 m/s) could be employed for surface acoustic wave devices.[3] Annealing is an important technique to understand the microstructure of materials. Besides, AlN films may be utilized at mediate or high temperatures in different atmosphere; hence, it is essential to investigate oxidation behavior of the films under those conditions. This is part of our systematic studies on oxidation/degradation of nitride films at high temperature under controlled atmosphere. In our previous research conductive nitride films, such as TiN,[4] CrN,[5] and ZrN[6] concerning the subject have been investigated, here dielectric AlN is the focal point.

Aluminum nitride would be oxidized to alumina (Al_2O_3) in oxidizing environment and the thermodynamically stable phase is α-Al_2O_3. Before reaching α-Al_2O_3, several intermediate phases might be present during oxidation of aluminum nitrides. Although quite a few studies concerned oxidation of aluminum nitride, most of them focused on the material either in the bulk [e.g., Refs.[7,8]] or powder [e.g., Refs.[9,10]] form; only a few of them considered the thin film material.[11–14] Among these studies focusing on thin films, only the environment of pure oxygen, air, or N_2/O_2 mixing gases but with a very small oxygen partial pressure range[14] has been considered. So far there is a lack of systematic studies on oxidation of AlN films under different atmospheres possessing, especially very different nitrogen and oxygen partial pressures. Furthermore, very few researches have been conducted on the microstructure evolution during oxidation or phase transformation in such a material.

The aim of this research is to investigate oxidation behavior of aluminum nitride thin films at high temperatures under controlled atmosphere with drastically different nitrogen/oxygen partial pressure ratios. Changes in microstructures during oxidation and phase transformation are also investigated.

2. Experiments

AlN films were reactively sputtered onto Si substrates by unbalanced magnetron sputtering deposition (Victor Taichung

* Corresponding author. Tel.: +886 4 22851455; fax: +886 4 22857017.
E-mail address: fhlu@dragon.nchu.edu.tw (F.-H. Lu).

0955-2219/$ – see front matter © 2007 Elsevier Ltd. All rights reserved.
doi:10.1016/j.jeurceramsoc.2007.07.015

Machinery, VVS-70L). The deposition parameters are given as follows: Al metal cathode (purity 99.999%), base pressure 2.7×10^{-4} Pa, working pressure 0.53 Pa, bias −315 V, current 6.4 A, N_2 flow rate 200 sccm, Ar flow rate 50 sccm, substrate temperature 190 °C, and deposition time 20 min. The resultant thickness of the film was about 480 nm, determined from cross-sectional micrographs of scanning electron microscope.

Subsequently, as-deposited AlN specimens were annealed over temperatures between 700 and 1200 °C in flowing gases within a gas-tight tube furnace equipped with a zirconia (15 mol% CaO-doped) O_2 sensor. The flowing gases included air, "pure" nitrogen (N_2, 99.999% purity), and forming gas [$N_2/H_2 = 9$, $H_2 = (10 \pm 0.2)\%$], which exhibited similar nitrogen partial pressure (p_{N_2}), but drastically different oxygen partial pressures (p_{O_2}). Values of p_{O_2} are 0.21 atm for air and $\sim 10^{-5}$ atm for "pure" nitrogen but are functions of temperature for $N_2/H_2 = 9$ (e.g., $\sim 10^{-24}$ atm at 700 °C and $\sim 10^{-16}$ atm at 1100 °C). The flow rate was controlled at about 200 sccm using a Unit 8100 mass flow meter. The pressure in the furnace was kept at about atmospheric pressure. The ramping rate was set at about 5 °C/min and the soaking time was varied from 2 to 12 h.

After oxidation, each specimen was firstly inspected under an optical microscope. The crystal structure of the film was determined by an X-ray diffractometer (MacScience MXP3) operated at 40 kV and 30 mA ($\lambda_{Cu,\ K\alpha} = 0.154$ nm) and a Raman scattering spectrometer (Jobin yvon TRIAX 550) with a 633 nm He–Ne laser operated at 25 mW power. The microstructure of the film was carefully examined by a field-emission scanning electron microscope (JEOL JSM-6700F) operated at 3 kV. An atomic force microscope (Seiko SPA 400) was also used to aide revealing the surface morphology after oxidation.

3. Results and discussion

The original color of as-deposited AlN films was dark reddish. After annealing, the color of AlN films would turn red-green or green, depending on the annealing temperature, time, and atmosphere. Degradation diagrams similar to those reported in our previous studies for TiN,[4] CrN,[5] and ZrN[6] were then generated by plotting the regions of color changes resulted from formation of different oxide phases occurring at various temperatures and times under controlled atmosphere; see Fig. 1(a) for air, (b) for N_2, and (c) for $N_2/H_2 = 9$ mixing gases.

3.1. Color change

After annealing, color changes of the films often indicate phase changes that primarily resulted from oxidation. Fig. 1 depicts the specific annealing times and temperatures at which color changes occurred in (a) air, (b) nitrogen, and (c) $N_2/H_2 = 9$ environment. Region I represents that no color change occurred, region II denotes films that turned red-green, and region III specifies films that became green. As shown in the figures, the boundary lines (dashed) between regions I (no color change) and II (red-green) as well as regions II and III (green) shifted

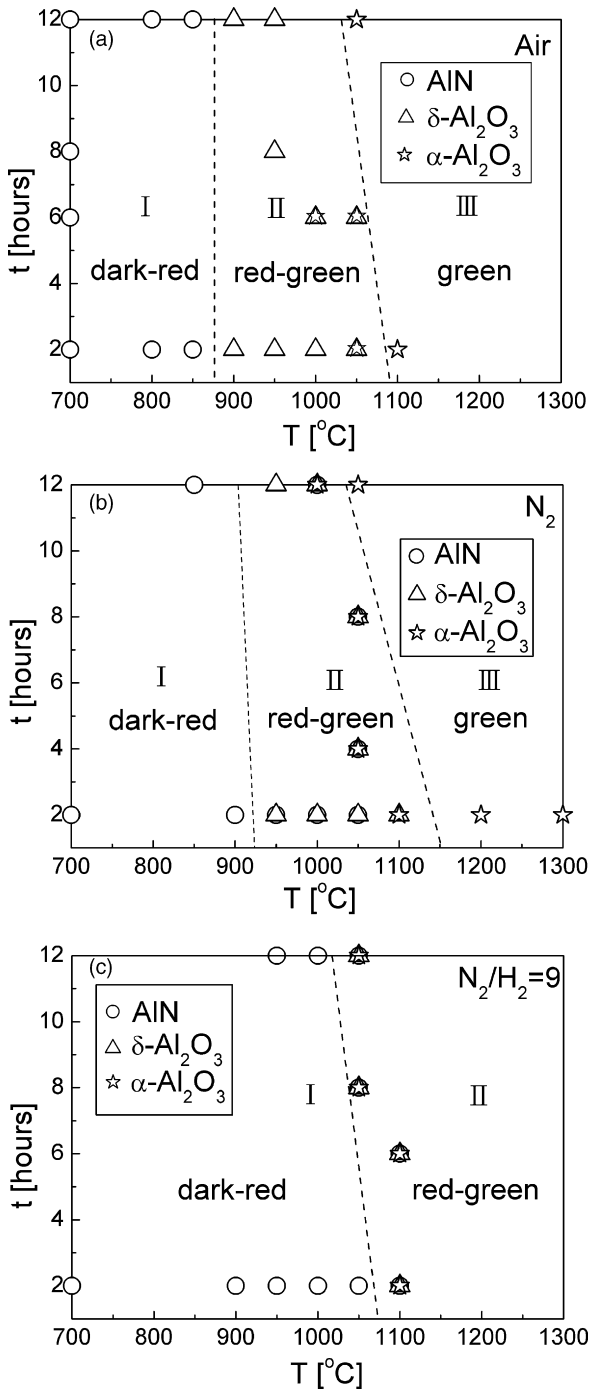

Fig. 1. Degradation diagram of AlN films annealed at various temperatures and times for (a) air, (b) N_2, and (c) $N_2/H_2 = 9$. The open round symbol (◯) denotes no color/phase change, triangle (△) and star (☆) represent formation of δ-Al_2O_3 and α-Al_2O_3, respectively.

toward higher temperatures and longer times when annealing was conducted from high to low oxygen-content environment. Actually there is no region II in $N_2/H_2 = 9$. This means that the severity of color change (oxidation) follows the sequence: air > N_2 > $N_2/H_2 = 9$ at the same annealing temperatures and times. The oxidation reaction for AlN can be written as:

$$\tfrac{4}{3}\mathrm{AlN} + \mathrm{O_2} = \tfrac{2}{3}\mathrm{Al_2O_3} + \tfrac{2}{3}\mathrm{N_2} \quad (1)$$

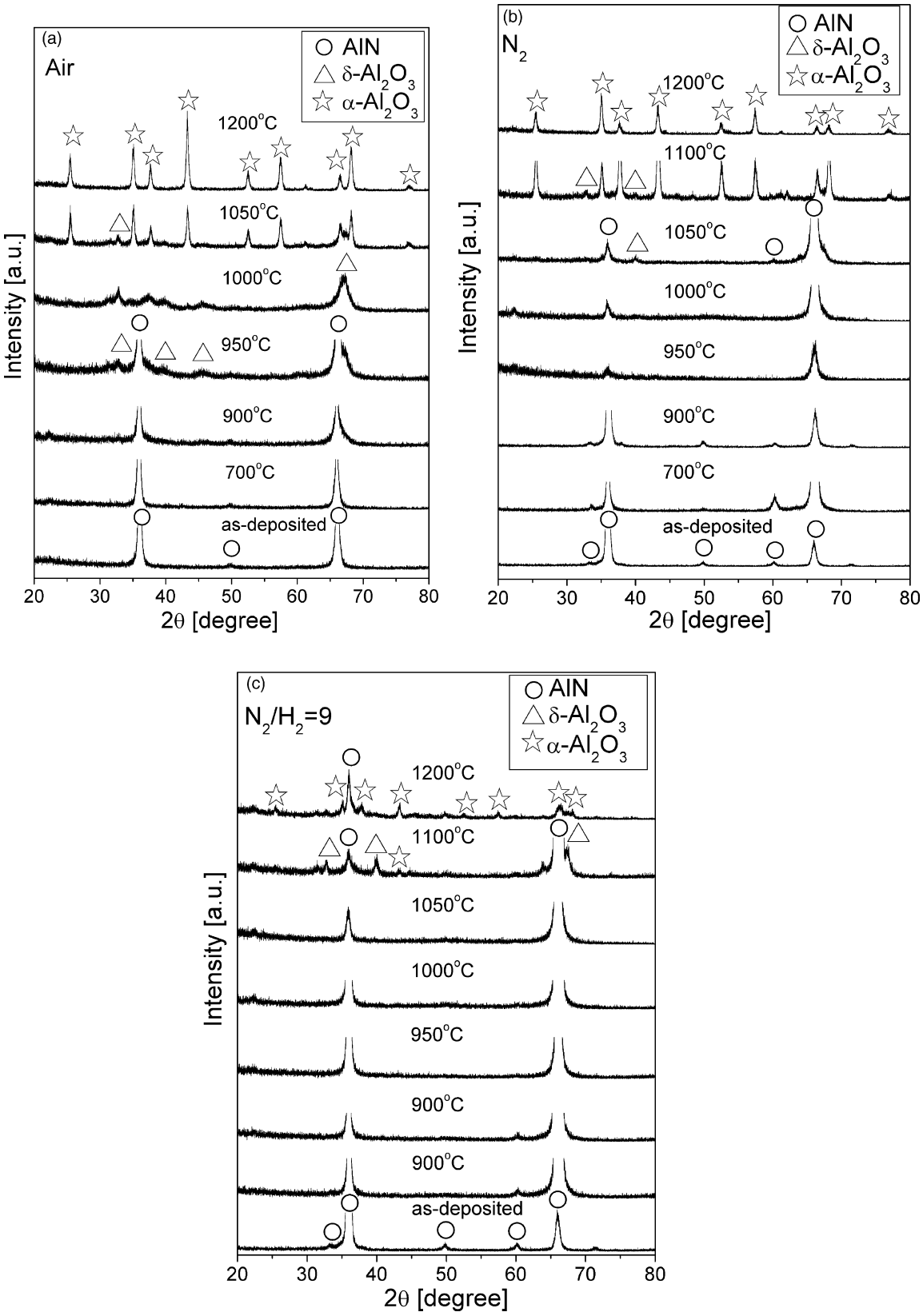

Fig. 2. X-ray diffraction spectra of as-deposited AlN films and the films annealed in (a) air, (b) N_2, and (c) $N_2/H_2 = 9$ at 700–1200 °C for 2 h.

The Gibbs free-energy change of the oxidation ΔG and the standard Gibbs free-energy change ΔG° are given below by summarizing the thermodynamic data from literature[15]:

$$\Delta G = \Delta G^\circ + RT \ln\left(\frac{p_{N_2}^{2/3}}{p_{O_2}}\right) = -RT \ln\left(\frac{p_{N_2}^{2/3}}{p_{O_2}}\right)_{equil.} + RT \ln\left(\frac{p_{N_2}^{2/3}}{p_{O_2}}\right) = [-690+0.064 \times T]+\frac{RT}{1000} \ln\left(\frac{p_{N_2}^{2/3}}{p_{O_2}}\right) \quad [kJ/mol] \quad (2)$$

where R is the gas constant, T the annealing temperature [K], and $(p_{N_2}^{2/3}/p_{O_2})_{equil.}$ is the specific nitrogen and oxygen partial pressure ratio at which AlN is in thermodynamic equilibrium with Al_2O_3. It is noteworthy that the thermodynamic data are valid for temperatures in the range of 327–1327 °C. It is clearly shown in the equation that the driving force of the oxidation depends on not only the annealing temperature but the nitrogen/oxygen partial pressure ratios of the annealing gases. The figures also show the data points that symbolized the films remained unchanged (◯) or underwent different phase changes (△: δ-Al_2O_3, ☆: α-Al_2O_3) that will be discussed in the next section.

3.2. Crystal structure

X-ray diffraction (XRD) was used to characterize the films prior to and after oxidation. Fig. 2 shows XRD spectra of as-deposited specimens and the specimens annealed from 700 to 1200 °C in (a) air, (b) nitrogen, and (c) $N_2/H_2 = 9$ gases for 2 h. As shown in the figures, as-deposited films exhibited wurtzite AlN characteristic diffraction peaks (JCPDS 25-1133[16]). It is noteworthy that as-deposited specimens exhibited a (0 0 2) preferred orientation.

To compare the oxidation behavior among those different atmospheres, relative peak integrated intensities of AlN, δ-Al_2O_3, and α-Al_2O_3, which were calculated by considering the strongest peak of each phase, i.e., AlN (0 0 2), δ-Al_2O_3 (0 2 2), and α-Al_2O_3 (1 1 3) as revealed in Fig. 2, were plotted against annealing temperature as given in Fig. 3 for (a) air, (b) nitrogen, and (c) $N_2/H_2 = 9$ gases. It is shown that tetragonal δ-Al_2O_3 peaks (JCPDS 46-1131[16]) started to appear at 950 °C in air, and showed up at a higher temperature 1050 °C in N_2 while could not be found until 1100 °C in $N_2/H_2 = 9$. Rhombohedral α-Al_2O_3 peaks (JCPDS 46-1212[16]) were observed above 1000 °C in air, 1100 °C in N_2 and $N_2/H_2 = 9$. Complete oxidation occurred at 1000 °C in air and at 1200 °C in N_2, while only slight oxidation could be observed in $N_2/H_2 = 9$ even at 1200 °C. Apparently both oxidation of AlN and phase transformation of resultant alumina depend on not only the temperature but the oxygen partial pressure. It is not hard to understand that beside temperature, oxygen partial pressure would also affect greatly the degree of oxidation as predicted by above thermodynamic considerations, as given in Eqs. (1) and (2). Fig. 4 shows the plot of the relative peak integrated intensity

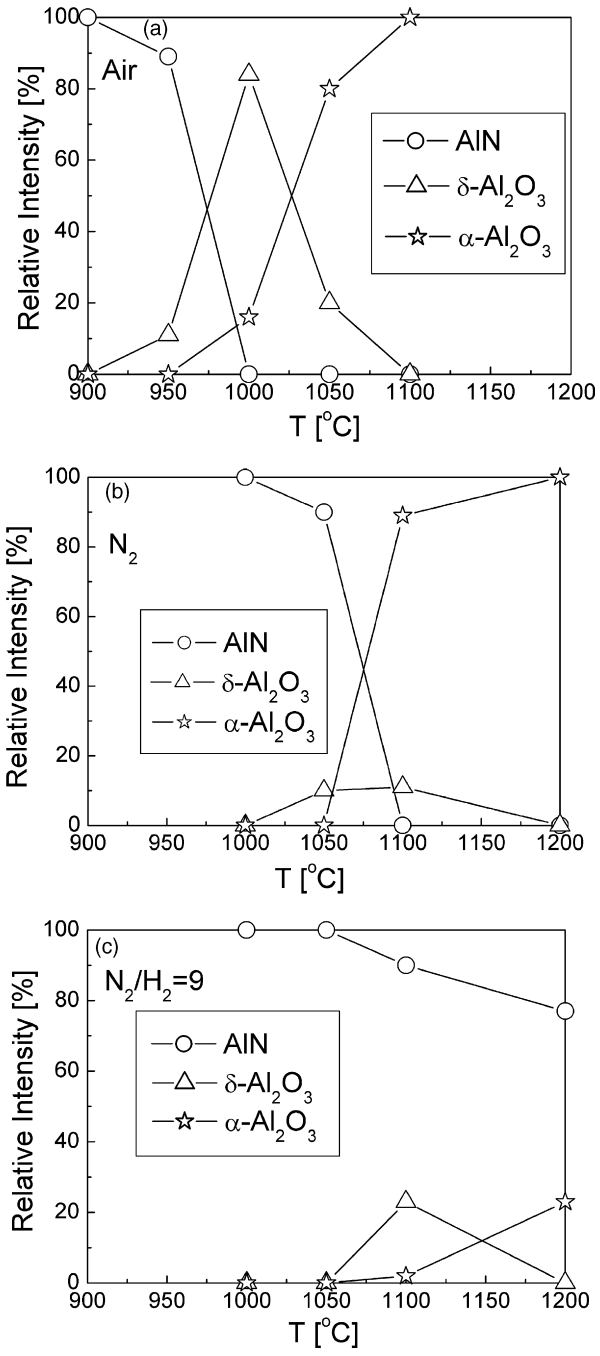

Fig. 3. Relative peak integrated intensities of AlN, δ-Al_2O_3, and α-Al_2O_3 in (a) air, (b) N_2, and (c) $N_2/H_2 = 9$, deduced from Fig. 2, as a function of annealing temperature.

of overall Al_2O_3 (delta and alpha phases) versus logarithm of nitrogen and oxygen partial pressure ratio at fixed temperatures of 950, 1000, and 1050 °C. The vertical lines represent the specific ratio $(p_{N_2}^{2/3}/p_{O_2})_{equil.}$ at which AlN is in thermodynamic equilibrium with Al_2O_3 at a given temperature. These ratios were evaluated from Eq. (2). For a given flowing gas with a specific p_{N_2}/p_{O_2} ratio, the relative peak integrated intensity of Al_2O_3 increased rapidly with temperature. On the other hand, at a fixed temperature, the relative intensity of the oxide

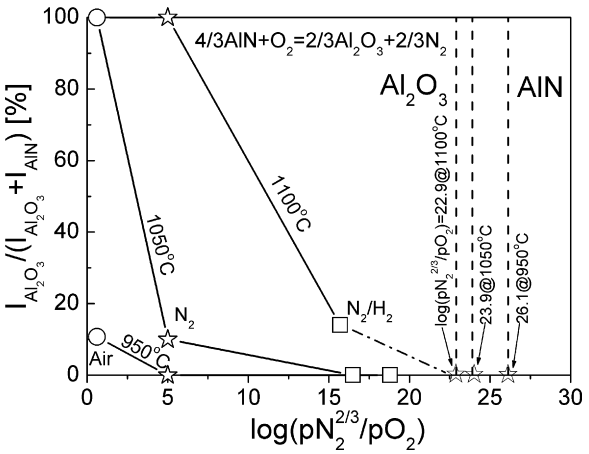

Fig. 4. Relative peak integrated intensity of Al_2O_3 versus logarithm of nitrogen and oxygen partial pressure ratio in different atmospheres at fixed temperatures of 950, 1050, and 1100 °C. The vertical lines represent the specific nitrogen and oxygen partial pressure ratio at which AlN is in thermodynamic equilibrium with Al_2O_3.

decreased drastically with increasing p_{N_2}/p_{O_2} ratio. Consider at a given temperature, say, 1050 °C, the Gibbs free-energy changes of oxidation, ΔG, calculated by using Eq. (2) were $\Delta G(\text{air}) = -602\,\text{kJ/mol} < \Delta G(N_2) = -581\,\text{kJ/mol} \ll \Delta G(N_2/H_2 = 9) = -491\,\text{kJ/mol}$. This thermodynamic prediction is clearly consistent with the trend of color changes as stated earlier and of the degree of oxidation concerning the relative intensity of the oxide.

As for the phase transformation of alumina from a δ-phase into a α-phase, no research has been reported concerning how the atmosphere, i.e., nitrogen/oxygen partial pressures would affect the transformation. This would be further explored by investigating microstructure changes and constituents of resultant oxides in different nitrogen/oxygen ratio environment.

3.3. Microstructure

Since AlN films are dielectric materials, field-emission scanning electron microscopy (FE-SEM) operated at low voltages could be used to examine changes in microsctructures prior to and after oxidation of AlN films. Fig. 5 shows the morphology of (a) as-deposited films and the films after oxidation at (b) 700 °C, (c) 850 °C, (d) 900 °C, (e) 950 °C, (f) 1000 °C, (g) 1050 °C, and (h) 1100 °C for 2 h in air. Below 700 °C, the morphology of the films was rather similar, i.e., remaining a nano-particulate structure. The grain size was about 30 ± 5 nm. Between 700 and 900 °C, the grain boundary became more blurred with increasing temperature although no oxide phase could be discerned by XRD. Larger oxidant irregular grains over 100 nm were present above 950 °C. It is noteworthy that at 1050 °C two types of morphologies denoted zones A and B, as shown in Fig. 5(g), appeared, indicating existence of two phases. Zone A shows similar microstructures of the films oxidized at 950–1000 °C while zone B reveals much denser/smoother surface like a sintering body with several nanopores. Crystalline phases for these two regions will be resolved by micro-Raman spectroscopy and discussed later. The microstructure evolution of oxidation in N_2 and $N_2/H_2 = 9$ was quite similar to that in air except oxidation would be hindered with increasing p_{N_2}/p_{O_2}.

Abovementioned two types of microstructures were revealed in Fig. 6(a) with a much smaller scale. From such a micrograph two different areas were clearly identified; the grey area with blurred boundaries referred to zone A while the dark area with distinct boundaries indicated zone B, as given in Fig. 5(g). Annealing the films in $N_2/H_2 = 9$ at 1200 °C for 2 h resulted in similar microstructures except much denser surface was observed for zone B, as shown in Fig. 6(b). Crystalline phases for those different zones could be easily identified by micro-Raman spectroscopy using δ- and α-Al_2O_3 powders as references. Micro-Raman spectra of these two zones at various temperatures under different atmosphere and reference powders are depicted in Fig. 6(c and d). Zone A with irregular grains/rough surface was identified as δ-Al_2O_3 while zone B with dense structure/smooth surface was α-Al_2O_3. Transforming from δ into α phase caused a volume shrinkage, which could be easily revealed by atomic force microscopy, as revealed in Fig. 7. The volume shrinkage after phase transformation might be due to both much higher density of α-alumina ($D_{\delta\text{-}Al_2O_3} = 2.97\,\text{g/cm}^3$, $D_{\alpha\text{-}Al_2O_3} = 3.99\,\text{g/cm}^3$)[16] and sintering effect in the α-alumina. The existence of many tiny pores as shown in Fig. 5(h), which disappeared at higher temperatures, provides another evidence of sintering effect. The results for different atmospheres all reveal similar phase changes during transformation.

Taking 1050 °C at which two oxide phases coexisted in all atmospheres as an example to investigate how nitrogen/oxygen partial pressures affect the phase transformation. Fig. 8 shows the ratio of relative amount of α-Al_2O_3, which was evaluated by averaging five areas for each specimen with a commercially available imaging software, to that of overall oxidants as a function of oxidation time in different atmospheres. It is clearly shown that the trend of phase transformation in air is quite different from that in nitrogen and forming gas. According to the nucleation and growth theory for austenite–pearlite phase transformation,[17] rapid nucleation of the new phase would yield the decrease of the transformation rate with time while slow nucleation would cause the increase of the transformation rate. As shown in the figure, the slope for air is rather different from that for other atmospheres, indicating that transformation mechanisms might be different in diverse atmospheres. The fraction of transformed alumina in air obeys approximately (dashed line) the well-known Avrami, John–Mehl equation[18,19]

$$\Phi(t) = 1 - \exp\left(\frac{-t}{\tau}\right)^n \tag{3}$$

where n is a constant characteristic of the type of nucleation process and τ a time constant during the transition. Nevertheless, the data in N_2 and $N_2/H_2 = 9$ could not be fitted to the above equation (solid lines: spline fit). Thus, not too much scientific insight could be deduced from current limited results. This is worth being further explored.

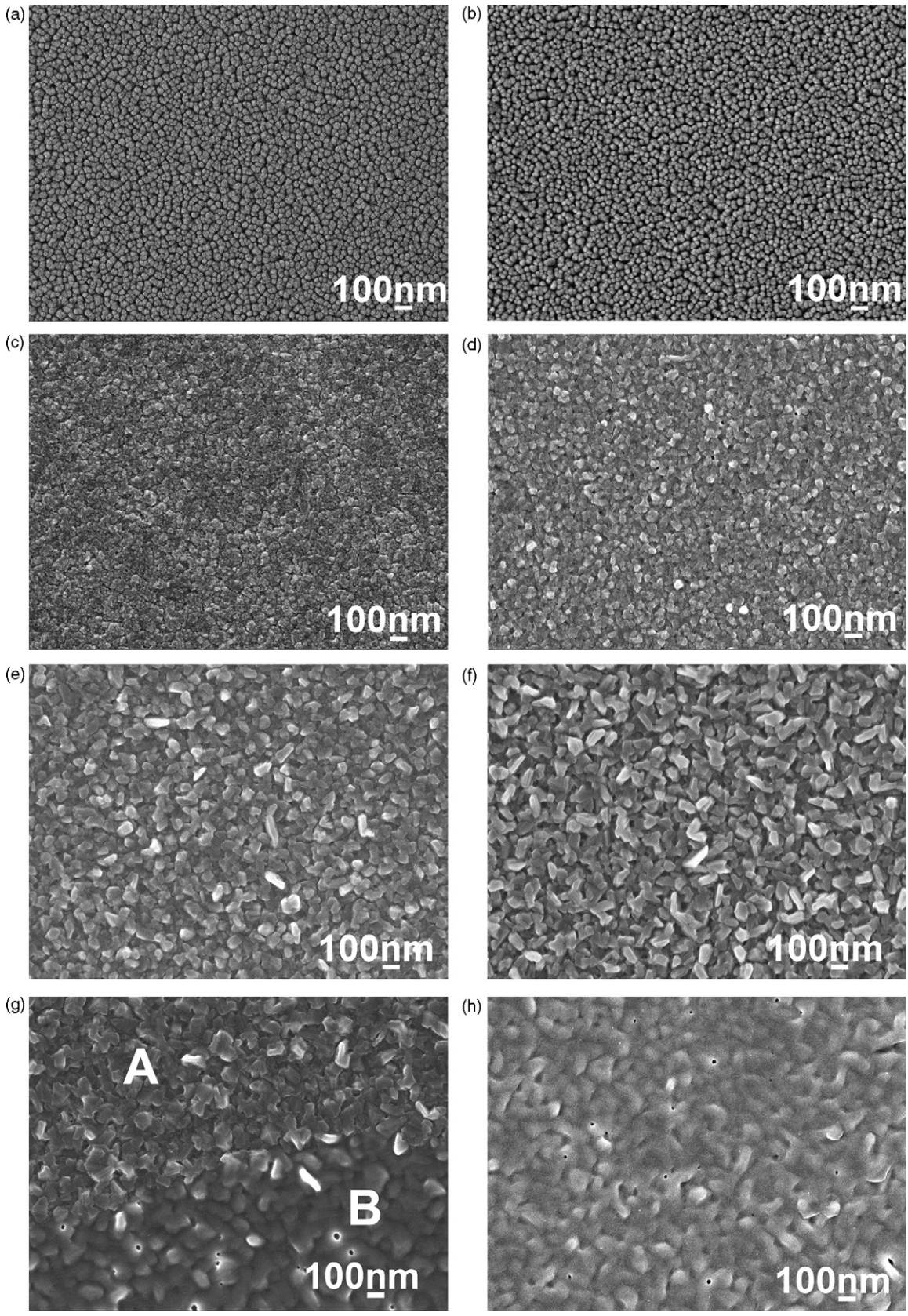

Fig. 5. Morphology of (a) as-deposited AlN films and the films oxidized in air for 2 h at (b) 700 °C, (c) 850 °C, (d) 900 °C, (e) 950 °C, (f) 1000 °C, (g) 1050 °C, (h) 1100 °C, revealed by field-emission scanning electron microscopy.

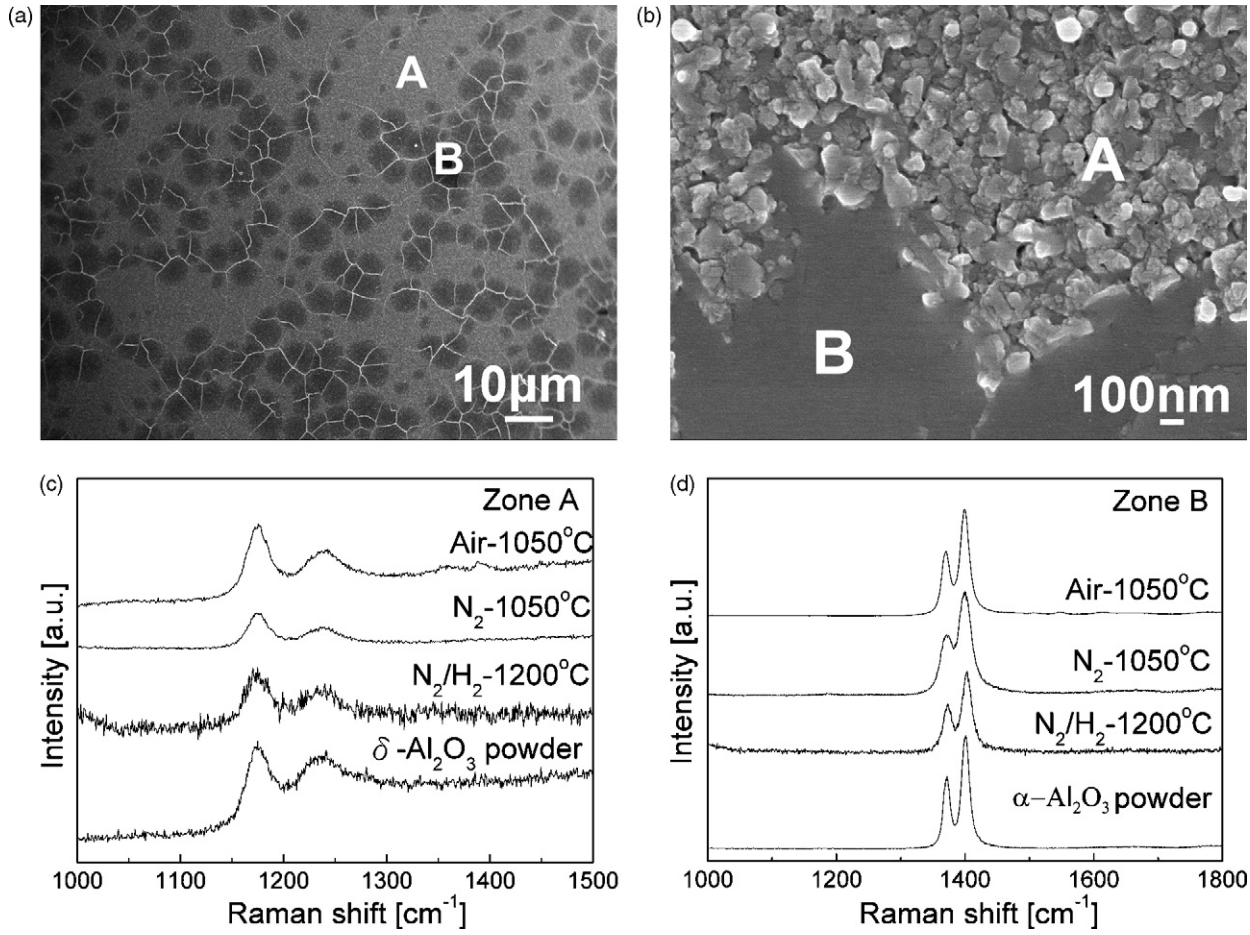

Fig. 6. Two typical distinct zones, denoted as A and B, after oxidation of AlN films for 2 h in (a) air (1000×) at 1050 °C and (b) $N_2/H_2 = 9$ (50,000×) at 1200 °C; micro-Raman spectra of (c) zone A (δ-Al_2O_3) and (d) zone B (α-Al_2O_3) in different atmospheres.

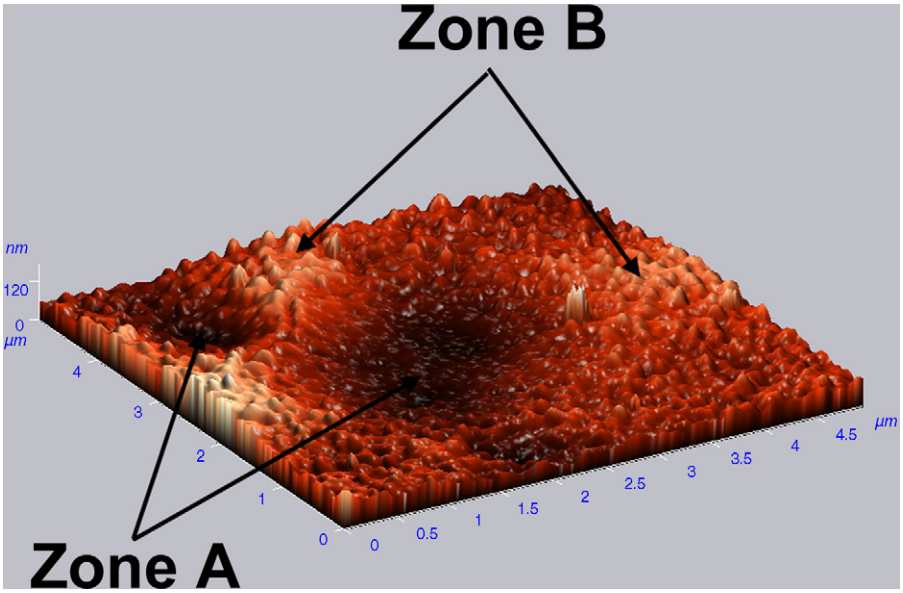

Fig. 7. Surface roughness of AlN films oxidized in air at 1050 °C for 2 h, revealed by atomic force microscopy. Zones A and B correspond to the regions shown in Fig. 6.

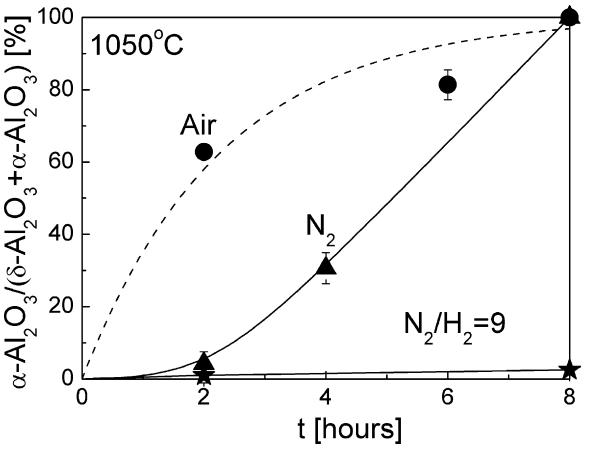

Fig. 8. Fraction of transformed α-Al_2O_3 as a function of oxidation time in different atmospheres. The trend in air is quite different from that in N_2 and $N_2/H_2 = 9$.

4. Conclusions

The degradation diagram has been generated for AlN films by plotting the regions of annealing temperatures and times at which the films has undergone phase changes in air, nitrogen, and forming gas ($N_2/H_2 = 9$), which possess drastically different nitrogen and oxygen partial pressures. The driving force of oxidation of the nitride film is the Gibbs free-energy changes. Different phases of oxidants including intermediate δ-Al_2O_3 and thermodynamically stable α-Al_2O_3 have been discerned by X-ray diffraction and micro-Raman spectroscopy. Not only the temperature but the nitrogen/oxygen partial pressures affect significantly the degree of oxidation of AlN and phase transformation in Al_2O_3.

Acknowledgments

This work is sponsored by the National Science Council of ROC (Taiwan) under Grant Number NSC 94-2216-E-005-004. We appreciate Dr. F.-S. Yen's research group at National Cheng Kung University for providing δ- and α-Al_2O_3 reference powders for Raman measurements. Thanks are also due to Victor Taichung Machinery (Taiwan) for helping preparation of aluminum nitride films.

References

1. Pierson, H. O., ed., *Handbook of refractory carbides and nitrides*. Noyes Publications, Westwood, New Jersey, 1996, pp. 209–247.
2. Yu, Y.-D., Hundere, A. M., Høier, R., Dunin-Borkowski, R. E. and Einarsrud, M.-A., Microstructure characterization and microstructural effects on the thermal conductivity of AlN(Y_2O_3) ceramics. *J. Eur. Ceram. Soc.*, 2002, **22**, 247–252.
3. Okano, H., Takahashi, Y., Tanaka, T., Shibata, K. and Nakano, S., Preparation of c-axis oriented AlN thin films by low-temperature reactive sputtering. *Jpn. J. Appl. Phys.*, 1992, **31**, 3446–3451.
4. Lu, F.-H., Feng, S.-P., Chen, H.-Y. and Li, J.-K., The degradation of TiN films on Cu substrates at high temperature under controlled atmosphere. *Thin Solid Films*, 2000, **375**, 123–127.
5. Lu, F.-H., Chen, H.-Y. and Hung, C.-H., Degradation of CrN films at high temperature under controlled atmosphere. *J. Vac. Sci. Technol. A*, 2003, **21**, 671–675.
6. Lu, F.-H. and Lo, W.-Z., Degradation of ZrN films at high temperature under controlled atmosphere. *J. Vac. Sci. Technol. A*, 2004, **22**, 2071–2076.
7. Robinson, D. and Dieckmann, R., Oxidation of aluminium nitride substrates. *J. Mater. Sci.*, 1994, **29**, 1949–1957.
8. Lee, J. W., Radu, I. and Alexe, M., Oxidation behavior of AlN substrate at low temperature. *J. Mater. Sci.*, 2002, **13**, 131–137.
9. Suryanarayana, D., Oxidation kinetics of aluminum nitride. *J. Am. Ceram. Soc.*, 1990, **73**, 1108–1110.
10. Brown, A. L. and Norton, M. G., Oxidation kinetics of AlN powder. *J. Mater. Sci. Lett.*, 1998, **17**, 1519–1522.
11. Ansart, F., Ganda, H., Saporte, R. and Traverse, J. P., Study of the oxidation of aluminum nitride coatings at high temperature. *Thin Solid Films*, 1995, **260**, 38–46.
12. Chowdhury, E. A., Kolodzey, J., Olowolafe, J. O., Qiu, G., Katulka, G., Hits, D. *et al.*, Thermally oxidized AlN thin films for device insulators. *Appl. Phys. Lett.*, 1997, **70**, 2732–2734.
13. Kolodzey, J., Chowdhury, E. A., Qui, G., Olowolafe, J., Swann, C. P., Unruh, K. M. *et al.*, Effects of oxidation temperature on the capacitance-voltage characteristics of oxidized AlN films on Si. *Appl. Phys. Lett.*, 1997, **71**, 3802–3804.
14. Wang, F., Zhang, R., Xiu, X. Q., Lu, D. Q., Gu, S. L., Chen, B. *et al.*, Study of dry oxidation of aluminum nitride on Si(1 1 1) substrate grown by metalorganic chemical vapor deposition. *Surf. Rev. Lett.*, 2003, **10**, 625–628.
15. Barin, I. and Platzki, G., ed., *Thermochemical data of pure substances*. 3rd ed. VCH, New York, 1995.
16. *Powder diffraction file. PDF-2 CDROM*. International Center for Diffraction Data, Newtown Square, PA, 2000.
17. Shewmon, P. G., *Transformation in metals*. J. Williams Book Company, Jenks, 1983, pp. 228–230.
18. Avrami, M., Kinetics of phase change I. *J. Chem. Phys.*, 1939, **7**, 1103–1112.
19. Johnson, W. A. and Mehl, R. F., Reaction kinetics in processes of nucleation and growth. *Trans. AIME*, 1939, **135**, 416–458.